Alma Mater Studiorum · Università di Bologna

Scuola di Scienze
Dipartimento di Fisica e Astronomia
Corso di Laurea in Fisica

Single-sided NMR to characterize cartilage tissue: a multi-parameter approach

Relatore:
Dott. Leonardo Brizi

Correlatore:
Dott. Carlo Golini

Presentata da:
Leonardo Conti

Anno Accademico 2021/2022

A Sara

Abstract

Questo lavoro di tesi è uno sviluppo del precedente lavoro del dott. Carlo Golini "A single-sided NMR approach to study structural differences of bovine articular tissue" e ne riprende le metodologie per confermarne ed approfondirne i risultati.
La ricerca è stata condotta mediante uno studio multiparametrico di risonanza magnetica nucleare (NMR) utilizzando uno strumento portatile (single sided) su campioni di tessuto cartilagineo bovino. Sono stati misurati quattro parametri: il tempo di rilassamento longitudinale T_1, il tempo di rilassamento trasversale T_2, il coefficiente di diffusione D dell'acqua nella matrice extracellulare cartilaginea ed il coefficiente α legato al rapporto del segnale dato dagli atomi di idrogeno (^{1}H) presenti nelle macroproteine rispetto al segnale dovuto a quelli presenti nelle molecole d'acqua.
L'obiettivo di questo lavoro di tesi è la verifica della capacità della strumentazione NMR portatile di distinguere la diversa morfologia degli strati che compongono il tessuto cartilagineo. Ciò è stato fatto mediante la determinazione del set multiparametrico acquisito tramite una procedura semi automatizzata. La finalità è la caratterizzazione del segnale di risonanza magnetica in funzione dei cambiamenti morfologici della cartilagine.
I risultati ottenuti confermano la possibilità di utilizzare questo tipo di indagine per correlare le variazioni del segnale NMR ai cambiamenti morfologici e composizionali del tessuto e quindi aprire la strada allo sviluppo di tecniche non invasive ed economicamente convenienti per la diagnosi di patologie che affliggono il tessuto cartilagineo come, ad esempio, l'osteoartrosi.

Contents

Chapter 1

Introduction

The study of nuclear magnetic resonance of ^{1}H nuclei (from here on NMR) has been shown to be more informative [1] than the standard radiography when investigating articular cartilage tissue. The reason for this is that time domain NMR allows to acquire information on hydrogenated fluid molecules and their interaction with the chemical-physical environment where they lay. When studying cartilage most of the signal is given by ^{1}H nuclei found in water molecules confined inside the tissue.
According to the 2019 Global Burden of Disease study (GBD) [2] [3], osteoarthritis is responsible for 2% of the total YLD (years of life with disability) and affects 7% of the global population, 48% more cases than registered in 1990. It is widely regarded by the available literature [4] that an early detection of the disease would allow the possibility of developing more efficient and targeted therapies.
The use of NMR-based techniques to diagnose osteoarthritis has been shown to be promising in a spectroscopy approach for the identification of biomarkers [5], in a parametric approach [6] and by imaging (MRI) of the affected tissues [7]. The main perks of NMR over other techniques are its non-invasiveness, allowing for in vivo studies, the use of non-ionizing radiation, multi-planar capabilities and soft tissue contrast.
The employment of a single-sided NMR instrument would be both economically and spatially advantageous, therefore more widely applicable which would lead to earlier diagnoses. Furthermore, when compared to conventional high field NMR apparata, it is clear that single sided instruments would be more comfortable for patients due to the fact that they can be easily manipulated and moved to the

position of interest without full body constriction.
Articular cartilage is divided into four main layers composed by varying relative quantities of water, collagen (mostly type II collagen), proteoglycans, chondrocytes of varying shapes and dimensions and other less prominent components. The collagen is present in the form of fibrils which compose, together with proteoglycans, the extra cellular matrix (ECM). The calcified layer is the closest to the bone. The deep layer sits above the calcified, in this region the collagen fibrils are perpendicular to the bone surface. The superficial layer (or tangential layer) is the closest to the surface and the collagen fibrils in this zone are parallel to the bone surface. The middle layer, situated between the deep and superficial ones, contains fibrils which are orientated obliquely providing an anatomic bridge between the deep and the superficial layers [8]. Water,which makes up 80 % of the wet weight in the superficial layer to 65 % in the deep layer, can be found both as a gel (specifically in the intrafibrillar space) and as a liquid. [8]
This work focuses on the use of portable single-sided instruments to determine sequences and parameters that are capable of discriminating the main characteristics of healthy cartilage with the ultimate goal of studying them on degraded samples and eventually linking them to the clinical course of osteoarthritis.

Chapter 2

Materials and methods

2.1 Sample

This section contains the most relevant information in the context of this work about articular cartilage and how the various samples were treated to obtain minimal dehydration.

2.1.1 Sample description

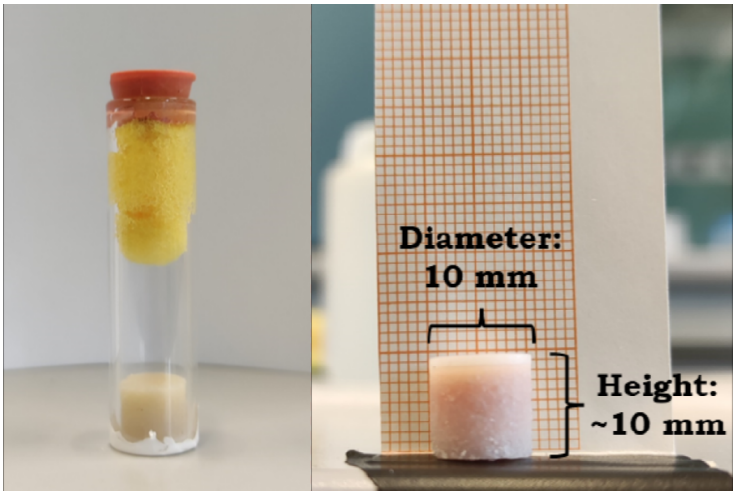

Figure 2.1: *Left: sample inside the test tube with sponge at the top and teflon at the bottom. Right: close up of a sample. Images taken from Carlo Golini, "A single-sided NMR approach to study structural differences of bovine articular tissue" , 2023*

The samples used were obtained in the Laboratory of Medical Technology of the Rizzoli Orthopedic Institute from bovine knee joints. The samples obtained are of cylindrical shape, with an height of about 10 mm (up to 3 mm of cartilage with the rest being bone) and a diameter of 10 mm as shown in figure 2.1.
For this work measures have been performed on twelve samples of bovine articular cartilage : ten of these were obtained from tibiae and the other two from femora. Partial data from two other data sets (the first with ten femora and ten tibiae, the second with ten femora and eight tibiae) were used to compare the resulting parameters for the middle layer.

2.1.2 Sample conservation and preparation

To prevent dehydration and achieve the most resemblance to the in vivo condition, the samples have been individually wrapped in a gauze imbued with a water and Phosphate Buffered Saline (PBS) solution and then stored in a freezer inside glass test tubes. The thawing process (performed only once per sample) happens inside the water and PBS solution to minimize air exposure. Right after thawing the samples are first dried, then placed in a cylindrical glass tube with teflon (commercial denomination for polytetrafluoroethylene) on the end that will lay closest to the NMR-MOUSE and sponge imbued with the aforementioned PBS solution on the other (see figure 2.1).

2.2 Fundamental NMR notions

The phenomenon of nuclear magnetic resonance involves the interaction of an atomic nucleus with an external magnetic field $\mathbf{B_0}$ which will be referred as the polarization field. The so called Zeeman effect takes place, causing a splitting in energy levels proportional to the nuclear magnetic momentum of the nucleus $\boldsymbol{\mu}$. If the atom subjected to the polarization field has no angular momentum then its nuclear magnetic momentum takes the form of [9]

$$\boldsymbol{\mu} = \gamma_n \hbar \mathbf{S} \tag{2.1}$$

where $\mathbf{S}$ is the spin angular momentum of the nucleus and $\gamma_\mathbf{n}$ is its gyromagnetic

ratio. The entity of the splitting of the energy levels is described by the following

$$E = -\boldsymbol{\mu} \cdot \mathbf{B_0} \tag{2.2}$$
$$= -\gamma_n \hbar \mathbf{S} \cdot \mathbf{B_0} \tag{2.3}$$

It can be deduced that for a particle of spin $\frac{1}{2}$ such as a proton the difference between the two different energy levels is $\Delta E = \gamma_n \hbar \mathbf{B_0}$.
Using then the Planck-Einstein relation for the energy carried by a photon $E = hf$ where f is the frequency of the photon it can be seen that the photon emitted (or absorbed) in a transition between two energy states in a Zeeman effect setting is

$$\Delta E = \gamma_n \hbar \mathbf{B_0} = hf \tag{2.4}$$
$$\therefore \quad \omega_0 = 2\pi f = \gamma_n \mathbf{B_0} \tag{2.5}$$

ω_0 is known as the Larmor frequency. Since the NMR experiments for this work have been performed on samples with a large number of particles it is now appropriate to study the ensamble behaviour.
Let $\mathbf{M}$ be the net nuclear magnetization vector, its modulus can be defined by the following relation [10]

$$M = -\frac{U}{\mu B_0} \tag{2.6}$$

where U is the total energy of a system of non-interacting spins and B_0 is the modulus of the polarization field which will be assumed to be parallel to the z-axis direction. Since the nuclei taken into consideration for the NMR experiments performed have spin $\frac{1}{2}$ the modulus of $\mathbf{M}$ can be expressed as [10]

$$M = N_\uparrow - N_\downarrow \tag{2.7}$$

where $N_{\uparrow/\downarrow}$ is the number of nuclei with $m_s = \pm\frac{1}{2}$.

Given these definitions it can be shown that the following Curie law for the magnetization at equilibrium holds

$$M_0 = NB_0 \frac{\gamma_n^2 \hbar^2 S(S+1)}{3k_B T} \tag{2.8}$$

At equilibrium the magnetization vector is parallel to the polarization field [9]. The time evolution of the magnetization vector is described by

$$\frac{d\mathbf{M}}{dt} = \gamma_n \mathbf{M} \times \mathbf{B_0} \tag{2.9}$$

which defines a precession of $\boldsymbol{\mu}$ along $\mathbf{B_0}$ with frequency equal to the Larmor frequency. While the system returns to equilibrium it emits electromagnetic waves which make up the signal acquired in an NMR experiment.
Tilting $\boldsymbol{\mu}$ from its equilibrium orientation and thus giving start to the precession motion is achieved by applying a second polarization field, denoted $\mathbf{B_1}$, orthogonal to $\mathbf{B_0}$, with frequency equal to the Larmor frequency : as shown in equation 2.5 this is the resonating condition for the system. The nutation angle α reached is directly proportional to the length of time t the system undergoes the application of the $\mathbf{B_1}$ field

$$\alpha = \gamma_n \mathbf{B_1} t \tag{2.10}$$

In order to study how the system returns to equilibrium it is costumary to solve equation 2.9 in a reference system rotating with frequency equal to the Larmor frequency, thus obtaining the following Bloch equations for the magnetization's longitudinal component M_z and transverse component M_{xy} [9]

$$\frac{dM_z(t)}{dt} = -\frac{(M_z(t) - M_0)}{T_1} \tag{2.11}$$

$$\therefore \quad M_z(t) = M_z(0)e^{-\frac{t}{T_1}} + M_0(1 - e^{-\frac{t}{T_1}}) \tag{2.12}$$

$$\frac{dM_{xy}}{dt} = -\frac{M_{xy}}{T_2} \tag{2.13}$$

$$\therefore \quad M_{xy}(t) = M_{xy}(0)e^{-\frac{t}{T_2}} \tag{2.14}$$

T_1 and T_2 are respectively the longitudinal and transverse relaxation times and can

be used (among other parameters) to discern different materials. The process of longitudinal relaxation is strictly related to the redistribution of the spins' energies in order to reach the equilibrium condition given by the Boltzmann distribution. This process is achieved by the exchange of energy between the spins and the lattice which in turn causes fluctuations in the molecules' local magnetic fields forcing the spins to in turn loose coherence. Transverse relaxation is only caused by a loss of coherence between the spins and thus is accelerated by longitudinal relaxation.
The following relation between T_1 and T_2 can be formally derived

$$T_2 \leq 2T_1 \quad \text{(theoretical limit)} \tag{2.15}$$

however $T_2 \leq T_1$ is the usual practical limit.

Self diffusion

Self diffusion (from here on diffusion) is a phenomenon which arises in any fluid constituted by the same molecular species where the molecules travel with random motion due to thermal excitation. The mean squared displacement can be found using Einstein's diffusion equation [11]

$$\langle \mathbf{r}^2(t) \rangle = \langle x^2(t) + y^2(t) + z^2(t) \rangle = 6Dt \tag{2.16}$$

where D is the diffusion coefficient in absence of barriers.
In the context of NMR, and in the presence of a magnetic field gradient (such as the one provided by the NMR-MOUSE), the diffusion phenomenon causes a faster loss of coherence due to the variation of the Larmor frequency during the motion of the nucleus along the magnetic field gradient. The effect this has on acquired signal can be quantified as [11]

$$\frac{S(t = \Delta + \frac{2}{3}\delta)}{S_0} = e^{-\frac{t}{T_2}} e^{-\gamma_n^2 g^2 \delta^2 D(\Delta + \frac{2}{3}\delta)} \tag{2.17}$$

where g is the magnetic field gradient,δ is the encoding time and Δ is the diffusion time, both of which will be expanded upon in 2.4. If barriers that restrict diffusion are present, D is no longer independent of Δ and equation 2.16 no longer holds: in this condition and assuming that diffusion is happening inside a spherical pore of

radius R, the following relation is valid :

$$R = \sqrt{D\Delta} \tag{2.18}$$

which gives a way to evaluate R (or D) by means of NMR.
The following proportionality relation between D and the surface to volume ratio $\frac{S}{V}$ of the pore can also be derived if Δ is considered a constant parameter :

$$R \propto D \; ; \; \frac{S}{V} \propto \frac{1}{R} \tag{2.19}$$

$$\therefore \frac{S}{V} \propto \frac{1}{D} \tag{2.20}$$

2.3 The NMR-MOUSE

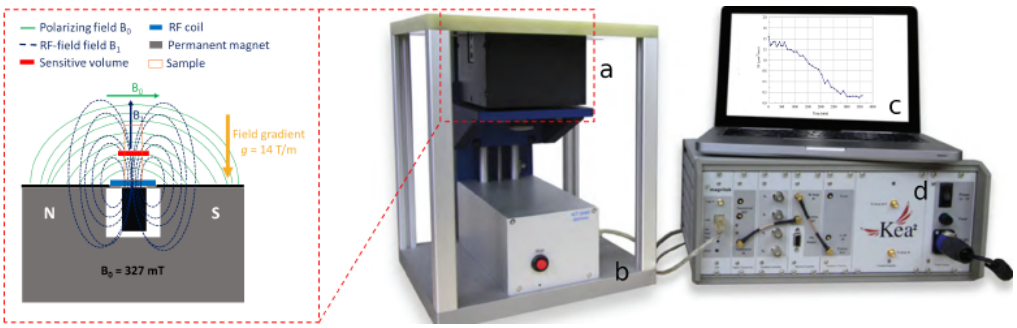

Figure 2.2: *Left: schematic representation of the NMR-MOUSE, the green lines represent the polarizing field B_0 while the dashed blue lines represent the r.f. field generated by the coil. The red rectangle represents the sensitive volume. Note that this does not accurately represent the configuration used in the experiment because 4 distancing slabs have been used so the coil should be closer to the sensitive volume. Right: replication of the experimental apparatus, the NMR-MOUSE (a) is mounted on a micrometer lift (b). The instrument is then connected to the Kea^2 spectrometer (d) controlled by a computer (c). Image taken from Carlo Golini, "A single-sided NMR approach to study structural differences of bovine articular tissue" , 2023*

The NMR-MOUSE (standing for Mobile Universal Surface Explorer) is a portable single sided NMR device designed by Blümitch et al. in 1996 [12]. The static magnetic field is provided by two U-shaped permanent magnets with anti-parallel magnetization that generate a polarization field B_0 (see 2.2). Between the magnets lies the radio frequency (RF) coil which serves as a transceiver for both sending RF

pulses and acquiring signal. The particular shape of the magnets also provides a strong and constant gradient g, perpendicular to the device's surface, for B_0.
The RF coil, responsible for the generation of the B_1 field, is built in a way such that it emits pulses with pulsation ω_0 and varying bandwidth $\Delta\omega = \frac{1}{t_p}$ where t_p is the time duration of the pulse (from here on referred to as pulse length). By virtue of this fact and equation 2.5 the width of the sensitive volume of the instrument, that is the volume where the spins are excited and spin relaxation takes place, can be determined :

$$\Delta\omega = \gamma B_0 + \gamma g \frac{\Delta y}{2} - (\gamma B_0 - \gamma g B_0) = \gamma g \Delta y \tag{2.21}$$

$$\therefore \quad \Delta y = \frac{\Delta\omega}{\gamma g} \tag{2.22}$$

It is important to note that, once ω_0 is selected, the position of the center of the sensitive volume is fixed and therefore, in order to be able to probe different depths inside a sample, it is necessary to move the RF coil : in order to do so the NMR-MOUSE is provided with distancing slabs 2 mms thick which can be placed between the magnets and the coil. For the measurements performed in this work only a configuration with 4 slabs has been used since, after testing, it provides the best signal to noise ratio (SNR). In the context of this work the sensitive volume has always been placed at a distance of 11 mm from the magnets where $B_0 = 0.327T$ and $\omega_0 = 13.9MHz$ thus giving, accounting for the distancing slabs placed, a maximum of about $3.1mm$ of penetration depth inside the sample.
The NMR-MOUSE has been mounted on a micrometer lift with step size of $50\mu m$ and the samples have been placed on a support base atop of it. The activity of the NMR-MOUSE is governed by the Kea^2 spectrometer which sends the necessary current pulses to produce the RF signals while also storing and amplifying the signal received.
The spectrometer is programmed via the Prospa software which enables the user to use predefined pulse sequences or to implement new ones by writing macros which are then compiled by the software. The user can also decide to implement a batch processing procedure which automates a series of NMR experiments. It is important to note that for the measurements performed in this work the predefined macros provided with the software have undergone a thorough overhaul which corrected critical issues with how some macros stored and elaborated the data from the

acquired signal which was not normalized over the number of "scans" (see section 2.4.1) performed and/or the "number of points" (see appendix A) acquired.

2.4 Pulse sequences

A pulse sequence is commonly defined as a series of r.f. pulses applied to a sample and the following detection of the NMR signal. In this section, after an introduction to the basic concepts and notation, the various sequences used in this work will be described.

2.4.1 Phase cycling and scans

Phase cycling is a common NMR technique employed in order to suppress parts of the NMR signal which are not of interest (e.g. couplings between the spins and noise generated by imperfections in the spectrometer) [9].
The signal emitted from the transmitter can be understood as follows :

$$s(t) \sim cos(\omega_0 t + \phi(t)) \tag{2.23}$$

where ω_0 is the same as in 2.3 and $\phi(t)$ is the radio-frequency phase. A "scan" is defined as one repetition of a pulse sequence with certain r.f. phases for every pulse used and the phase cycling technique consists in performing various scans with phases that depend on the experiments' objectives and then averaging the signal acquired over the number of scans performed.

2.4.2 Pulse sequence notation and diagram

A pulse sequence is commonly written in this notation:

$$[\theta_{\rho_1} - \tau_1 - (\alpha_{\rho_2} - \tau_2)_n - RT]$$

This fictitious sequence should be read as: a pulse with phase ρ_1 that achieves a nutation angle θ is applied and then an interval of time τ_1 elapses after which, for n times, the application of a second impulse α_{ρ_2} and elapsing of the interval τ_2 happens. RT stands for the repetition time of a sequence: it is fundamental in

order to perform a valid NMR experiment and taken as $5T_1$ in the context of this work.

Pulse sequences can also be described graphically via a diagram where the height of a column represents the nutation angle achieved. Figure 2.3 shows a representation of the sequence $[(\theta_{\rho_1} - \tau - \alpha_{\rho_2} - \tau)_2 - RT]$. It is important to note that generally the time is not in scale since the time of application of a pulse is orders of magnitude lower than the time between two pulses.

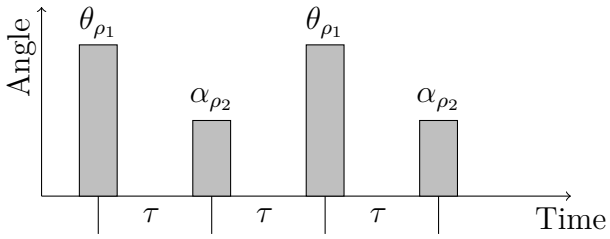

Figure 2.3: *Representation of the fictitious sequence* $[(\theta_{\rho_1} - \tau - \alpha_{\rho_2} - \tau)_2 - RT]$. *It is assumed that* $\theta = 2\alpha$. *Since it is preferable to keep the duration of the pulses constant the angle achieved, by equation 2.10, is directly proportional to the amplitude of the* $\mathbf{B_1}$

2.4.3 CPMG sequence

The Carr-Purcell-Meiboom-Gill (CPMG) sequence [13] is commonly used when it is necessary to suppress spin dephasing caused by the inhomogeneity of B_0 when investigating a sample with fluid components. In the context of this work the CPMG sequence, which reads as follows:

$$[\frac{\pi}{2}_x - (\frac{t_E}{2} - \pi_y - \frac{t_E}{2} - \text{Echo Acquisition})_n - RT] \tag{2.24}$$

is used to acquire a profile of the cartilage sample in order to determine at what depth the three layers lay. The trail of π pulses is used to refocus the spins in the sample and allows the detection of the signal since the free induction decay (FID) signal would decay too quickly. Acquisition is therefore performed n times ("Echo Acquisition" in 2.24), one for each refocus (or "echo") of the spins. The signal acquired is then fitted to the curve 2.14 in order to obtain a value for T_2.

It is also apparent that by virtue of the multiple echoes and acquisitions the sequence has a beneficial impact on the SNR of any signal detection: the CPMG

sequence has therefore been used at the acquisition phase of every pulse sequence in this work.

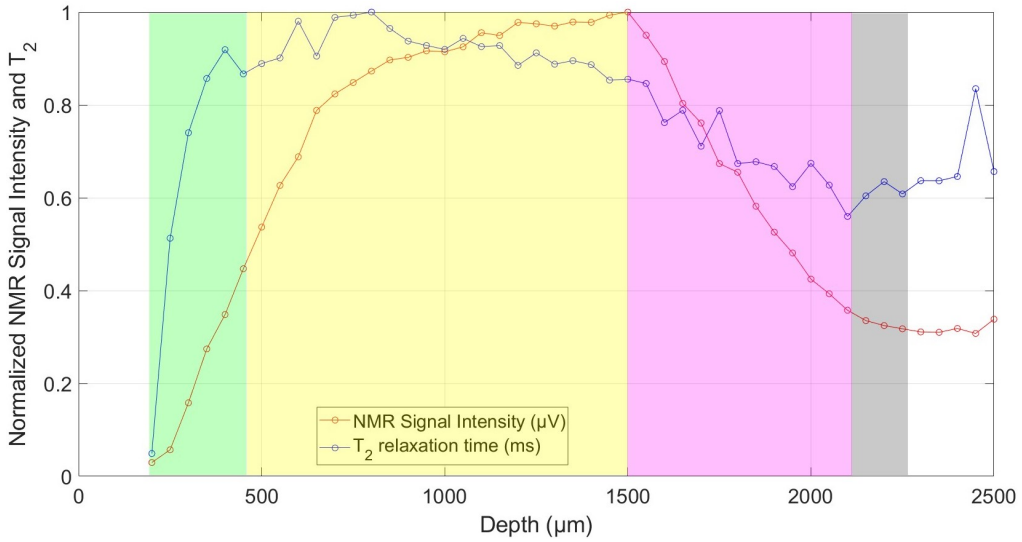

Figure 2.4: *Example of a sample's profile. Both the normalized signal intensity and T_2 curves are used to determine the depth of each layer. In green: the superficial layer, it is identified by positioning its end at half the signal intensity's steep rise, subsequent sequences have been performed at depth* 250 μm. *The middle layer is highlighted in yellow, it is identified by positioning its end at the point where the signal intensity and T_2 start to decrease, and subsequent sequences have been performed at depth* 1050 μm. *In purple: deep layer, identified by positioning its end at the minimum for T_2. subsequent sequences have been performed at depth* 1800 μm. *The calcified layer is highlighted in grey.*

To determine position and thickness of the three layers, a fast NMR profile of the sample is performed to acquire T_2 and NMR signal intensity (see figure 2.4). The results of the profile are then analysed and compared with documented anatomycal knowledge. The sensitive volume is moved via the micrometer lift by 50 μm steps and the sample undergoes the CPMG sequence at every step.
By the data presented in sections 2.1.1 and 2.3 the number of relevant steps is between 20 and 60 while ensuring that all the cartilage layers are distinguished.

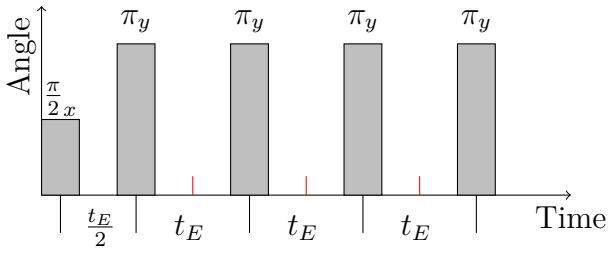

Figure 2.5: *Diagram for the CPMG sequence: the phase x is $\pi/2$ lower than y. t_E is known as "echo time" and signal acquisition is performed at times $t = nt_E$ and is represented as small red vertical lines. Pulses are applied to the sample at $t = (n + \frac{1}{2})t_E$.*

2.4.4 SR sequence

In this work the saturation recovery (SR) sequence has been used, as it is commonly done [14], to measure the longitudinal relaxation time T_1 of the samples by detecting the magnetization of the system at various recovery times t_{rec} and then fitting the obtained measures with the curve 2.13. The sequence used reads as follows:

$$[(\frac{\pi}{2})_m - \frac{\pi}{2} - t_{rec} - \frac{\pi}{2} - (CPMG*) - RT] \tag{2.25}$$

where "$(CPMG*)$" indicates that the CPMG sequence is performed as anticipated in section 2.4.3 without the initial $\frac{\pi}{2}$ which is already part of the SR sequence.
The m $\frac{\pi}{2}$ pulses (where m=5 for this work) are needed to take into account the inhomogeneity of B_1 and their purpose is to set $M_z(t_{rec} = 0) = 0$ in equation 2.13.

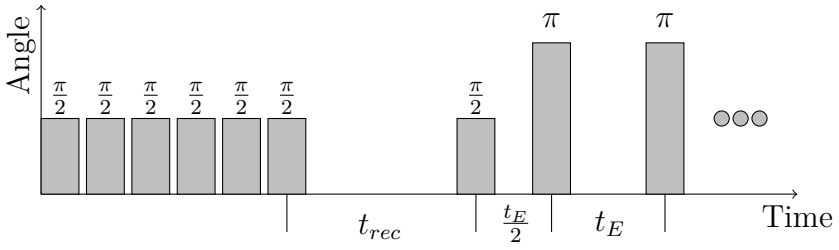

Figure 2.6: *Diagram for the SR sequence: five $\frac{\pi}{2}$ pulses to set $M_z(t_{rec} = 0) = 0$ are applied and then, after the application of another $\frac{\pi}{2}$ pulse, t_{rec} elapses. Various sequences with different t_{rec} are performed to track the magnetization's recovery.*

2.4.5 SSE sequence

The stimulated spin ehco (SSE) sequence is used to determine the self diffusion coefficient D in equation 2.17 which allows, by virtue of equation 2.18, the determination of the lenght scale of the cavities inside the sample. The sequence reads as follows:

$$[\frac{\pi}{2}_x - \delta - \frac{\pi}{2}_x - \Delta - \frac{\pi}{2}_x - \delta - \text{Echo acq} - (\frac{t_E}{2} - \pi_y - \frac{t_E}{2} - \text{Echo acq})_n - RT] \tag{2.26}$$

After the first two π pulses and the elapsing of the diffusion time Δ what follows is essentially a CPMG sequence where an echo acquisition after the $\frac{\pi}{2}$ pulse is added in order to measure $S(\Delta + \frac{2}{3}\delta)$ in equation 2.17 . S_0 is the signal acquired with $\delta = 0$ and the SSE sequence is performed various times with varying encoding time δ.

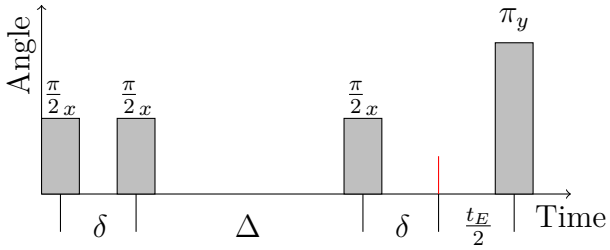

Figure 2.7: *Diagram for the SSE sequence. A red vertical line represents the moment the signal is acquired fpr the first time: the first echo forms after the last $\frac{\pi}{2}$ pulse (notice how this is not the case in the CPMG sequence) and it is the direct result of self-diffusion effects.*

2.4.6 DQ sequence

The double quantum (DQ) sequence [15] is performed to study ^1H residual dipolar couplings. The sequence reads as:

$$[\frac{\pi}{2}_{x+\Delta\phi} - \frac{\tau}{2} - \pi_{-x+\Delta\phi} - \frac{\tau}{2} - \frac{\pi}{2}_{x+\Delta\phi} - \frac{t_1}{2} - \pi_{-y} - \frac{t_1}{2} - \frac{\pi}{2}_y - \frac{\tau}{2} - \pi_{-y} - \frac{\tau}{2} - \frac{\pi}{2}_y - \tau_0 - (CPMG) - RT] \tag{2.27}$$

where τ is the conversion time, τ_0 is the filter time and t_1 is the evolution time. Leaving the CPMG part aside, the sequence can be divided in three parts: excitation, evolution and reconversion (see figure 2.8). During the excitation phase three pulses are sent in order to excite the motion of coupled spin pairs and then, during the evolution phase, a single pulse is applied to compensate for the inhomogeneity of B_0. During the reconversion phase three pulses are applied in order to convert the effects of the couplings into longitudinal magnetization. $\Delta\phi$ varies each time the sequence is repeated for the same τ, takes on four values: 0, $\frac{\pi}{2}$, π and $\frac{3\pi}{2}$ and is known as phase shift while t_1 and τ_0 respectively have been set to $50\mu s$ and $500\mu s$. In this work, the objective of the sequence is to measure the signal for relatively long τ (five points between $6ms$ and $500ms$) and then obtain the increase rate of the curve denoted as α.

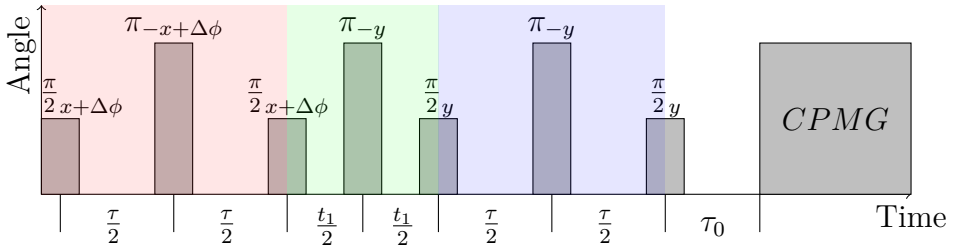

Figure 2.8: *Diagram for the DQ sequence: the phases x and y are the same used in the CPMG sequence and follow the same constraint. Highlited in red is the excitation phase, in green the evolution phase and in blue the reconversion phase. In the context of this work t_1 and τ are constant for all sequences performed.*

2.5 Kruskal-Wallis test

In order to determine whether or not the parameters obtained for different layers of cartilage were indeed dependent on the layer studied and not from the same statistical population the Kruskal-Wallis test [16] has been employed.
The test is performed under the assumptions that data comes from independent measures and that it follows the same continuous distribution (not necessarily normal, for which other tests like the ANOVA are more suited) and it compares the median values for the different populations on the notion that the data coming from the same population (having the same median value for each sample) is the null hypothesis.

In order to perform the test, given a number of samples C indexed by i such that $\sum i = C$, it is necessary to calculate the rank of the measures on a sample: by ordering these measures from lowest to highest rank = 1 is assigned to the lowest and it increases by one for every measure listed. Therefore, if n_i is the number of measures performed on the ith sample, the rank of those measures takes values from 1 to n_i.
Let $N = \sum n_i$ be the number of measures in all samples combined and R_i the sum of the ranks of the ith sample, the H factor is then defined as such:

$$H = \frac{12}{N(N+1)} \sum_{i=1}^{C} \frac{R_i^2}{n_i} - 3(N+1) \tag{2.28}$$

where large values of H lead to rejection of the null hypothesis.
Under the previous assumptions and if n_i is large enough ($n_i \geq 5$), the H factor follows the χ^2 distribution with $C - 1$ degrees of freedom: it can therefore be concluded that the p-value, which indicates the probability of measuring a larger H, can be used in order to reject the null hypothesis. The threshold value considered for p in this work is $p \leq 0.05$.
It is important to note that the Kruskal-Wallis test can only determine whether or not, for C sets of measures, at least two of them come from the same population: it is not a determination of which particular sets of measures come from the same population.

2.6 Box Plots and variability estimation

Box plots, or box-and-whisker diagrams, are a natural way for displaying data sets which are compared by their median value while not assuming that they follow any particular distribution. The data, once the outliers are excluded, is divided into four zones based on their percentile value with the median value represented by an horizontal line representing the median value (or 50th percentile), the "whiskers" lying on the 0th (or Q_0) and 100th (Q_4) percentile and the box containing the values between the box contains the values between the 75th (Q_3) and 25th (Q_1) percentiles. It is important to note that while it is not necessary that the median, Q_3 and Q_4 lines fall on a data point the whiskers always do in order to have a clear definition of the outlier data.

The use of box plots for data representation allows for the possibility to calculate an estimate of parameters' variability without assuming that they follow any particular distribution. Let the inter-quartile range, IQR_i, be the difference between the 75th percentile and 25th percentile values for the ith data set, V_{Max} equal to the maximum 100th percentile and V_{Min} equal to the minimum 0th percentile: an estimate for the variability of parameters' measures from the ith data set can therefore be computed as

$$IQR_{rel,i} = \frac{IQR_i}{V_{Max} - V_{Min}} \cdot 100\% \tag{2.29}$$

$IQR_{rel,i}$ is expressed as a percentage and the higher the value it assumes the wider is the IQR for the ith data set when compared to other data sets.

Chapter 3

Results and discussion

In this chapter the resulting parameters (T_1,T_2, D and α) from the NMR procedures will be shown and it will be determined whether the layers are distinguishable via these parameters. An ulterior comparison with two other data sets acquired with the same NMR procedures will be performed: in this context the three databases are labelled according to the order in which they were measured. For simplicity, the resulting parameters have not been grouped by the depth they have been measured at, since it depends on the overall thickness of the sample, but by the layer that was investigated.

3.1 Layer comparison

The following data has been collected from the aforementioned third batch of samples.
In Figure 3.1, the four NMR parameters determined by the procedures described in section 2.4 are depicted by box plot representation (see section 2.6). At first glance, almost all parameters have different behaviour in each cartilage layer.

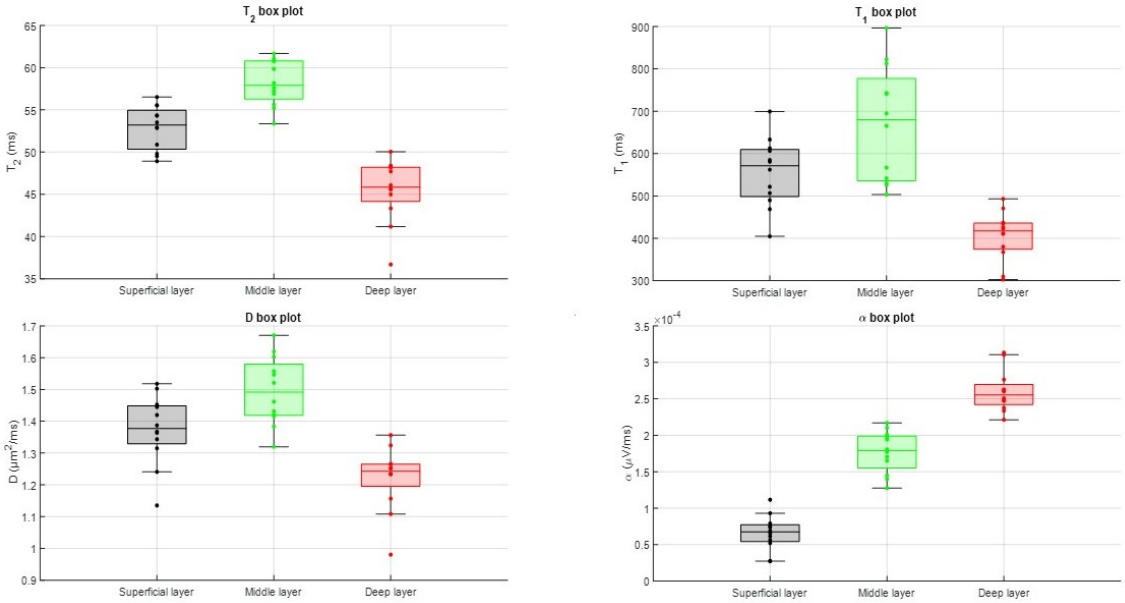

Figure 3.1: *Box plotting of the four parameters studied over the layer they have been measured at. Error bars are not present due to them being approximately the same length as the points' diameter. Top left: T_2 plot; top right: T_1 plot; bottom left: D plot; bottom right: α plot.*

Parameter	Layer	25th percentile	50th percentile	75th percentile
T_2 (ms)	superficial	50.3	53.2	54.9
	middle	56.3	57.9	60.8
	deep	44.2	45.9	48.2
T_1 (ms)	superficial	498	572	610
	middle	536	680	778
	deep	374	418	436
D $(\mu m^2/ms)$	superficial	1.33	1.38	1.45
	middle	1.42	1.49	1.58
	deep	1.20	1.24	1.27
α $(\mu V/s)$	superficial	0.05	0.07	0.08
	middle	0.16	0.18	0.20
	deep	0.24	0.26	0.27

Table 3.1: *Median, 25th and 75th percentile values measured for T_2, T_1, D and α for the three layers.*

Parameter	Layer	P-Value
T_2	superficial-middle-deep	$< \mathbf{10^{-4}}$
	superficial-middle	**0.0003**
	superficial-deep	$< \mathbf{10^{-4}}$
	middle-deep	$< \mathbf{10^{-4}}$
T_1	superficial-middle-deep	$< \mathbf{10^{-4}}$
	superficial-middle	**0.0496**
	superficial-deep	**0.0004**
	middle-deep	$< \mathbf{10^{-4}}$
D	superficial-middle-deep	$< \mathbf{10^{-4}}$
	superficial-middle	**0.0153**
	superficial-deep	**0.0022**
	middle-deep	$< \mathbf{10^{-4}}$
α	superficial-middle-deep	$< \mathbf{10^{-4}}$
	superficial-middle	$< \mathbf{10^{-4}}$
	superficial-deep	$< \mathbf{10^{-4}}$
	middle-deep	$< \mathbf{10^{-4}}$

Table 3.2: *Results of the Kruskal-Wallis test performed on the parameters obtained for the three layers. P-values lower than the threshold value 0.05 are in bold writing*

The data analysis by KW test of the parameters among the three layers and layer-by-layer (see Table 3.2) indicates that all the parameters are significantly different (p-value < 0.05). Only the comparison of T_1 between surface and middle layer shows a significance close to the reference threshold. The results, despite the small number of samples, confirm the trends analyzed on the two previous data sets (data not shown).

The relaxation times T_1 and T_2 and the diffusion coefficient D follow a similar trend between the layers having the highest median value for the middle layer and the lowest for the deep layer. The NMR signal relaxation of ^{1}H nuclei is sensitive to the chemical-physical environment in which the water molecules are confined. In light of equations 2.18 and 2.20 it can be inferred that, between the superficial and middle layer, the surface to volume ratio of structures of the ECM has increased. Moreover the parameter α, which is proportional to the ratio between low mobility ^{1}H and high mobility ones, increases over the sample's depth strengthening the hypothesis that the cartilage presents a more dense ECM and less water content

when going from the surface layer to the deep one.

Parameter	Layer	IQR	Max Value	Min Value	IQR_{rel}
T_2 (ms)	superficial	4.6	61.7	41.2	22%
	middle	4.5			22%
	deep	4.0			20%
T_1 (ms)	superficial	112	896	303	19%
	middle	242			40%
	deep	62			10%
D $(\mu m^2/ms)$	superficial	0.12	1.67	1.11	20%
	middle	0.16			29%
	deep	0.07			13%
α $(\mu V/s)$	superficial	0.03	0.31	0.03	11%
	middle	0.04			14%
	deep	0.03			11%

Table 3.3: *Third column: IQR for the parameters' distribution over the three layers. Fourth column: Highest 100th percentile. Fifth column: lowest 0th percentile. Sixth column: $IQR_{rel,i}$ as computed in equation 2.29, the i index is suppressed. $IQR_{rel,i}$ is taken to be indicative of the parameters' variability.*

By considering the weakest discriminant, the T_1 parameter between the superficial and the middle layer (see table 3.2), one can observe (see figure 3.1 and table 3.1) that T_1s of the middle layer show the highest variability among all parameters. This behaviour is confirmed by the results reported in table 3.3, where the relative variability (see section 2.6) of each parameter is estimated by computing the ratio between the IQR of each parameter among all layers and the difference between the maximum and minimum value for each parameter (excluding outliers). In fact, T_1 measures for the middle have the highest value of $IQR_{rel} = 40\%$, about 11% higher than the second highest being 29% for D in the middle layer (which, by inspecting table 3.2, is the weakest discriminant when excluding T_1).
As a general remark, the analyses indicated that the NMR parameters, obtained by the procedures used in this work, are good candidates for establishing robust estimators for cartilage tissue morphology by portable NMR instruments.

3.2 Database comparison

The following data has been gathered from all three batches and the main objective of the comparison is to validate the results obtained from the third batch of samples (the one studied in the previous section) and deduce possible links between the parameters and cartilage's morphology while excluding factors such as the animals' biological variability (i.e. sample's thickness, age, bone from which the sample was obtained etc.). This analysis focuses on the middle layer since it was found to be the one that can be identified with most consistency.

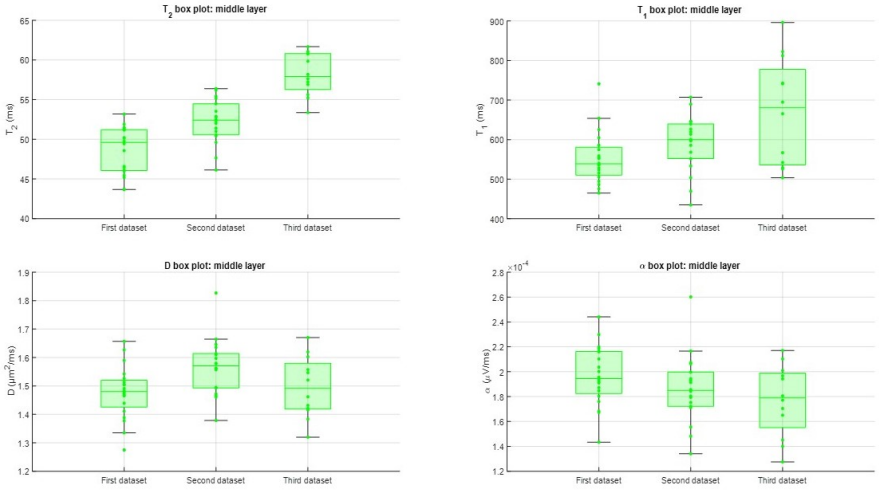

Figure 3.2: *Box plotting of the four measured parameters in the middle layer over the sample batch they have been determined from. The same representation conventions from 3.1 apply.*

Parameter	Layer	25th percentile	50th percentile	75th percentile
T_2 (ms)	first	46.1	49.6	51.2
	second	50.5	52.4	54.5
	third	56.3	57.9	60.8
T_1 (ms)	first	510	539	580
	second	552	600	640
	third	536	680	778
D $(\mu m^2/ms)$	first	1.43	1.48	1.52
	second	1.49	1.57	1.61
	third	1.42	1.49	1.58
α $(\mu V/ms)$	first	$1.8 * 10^{-4}$	$1.9 * 10^{-4}$	$2.2 * 10^{-4}$
	second	$1.7 * 10^{-4}$	$1.9 * 10^{-4}$	$2.0 * 10^{-4}$
	third	$1.6 * 10^{-4}$	$1.8 * 10^{-4}$	$2.0 * 10^{-4}$

Table 3.4: *Median, 25th and 75th percentile values measured for T_2, T_1, D and α in the middle layer for all three datasets*

Parameter	Database	P-Value
T_2	first-second-third	$\mathbf{< 10^{-4}}$
	first-second	**0.0009**
	first-third	$\mathbf{< 10^{-4}}$
	second-third	$\mathbf{< 10^{-4}}$
T_1	first-second-third	**0.0230**
	first-second	0.0574
	first-third	**0.0158**
	second-third	0.1755
D	first-second-third	**0.0376**
	first-second	**0.0130**
	first-third	0.6971
	second-third	0.0904
α	first-second-third	0.1665
	first-second	0.1520
	first-third	0.0942
	second-third	0.5534

Table 3.5: *Results of the Kruskal-Wallis test performed on the parameters obtained for the middle layer in the three data sets. P-values lower than the threshold value 0.05 are in bold writing*

By inspecting figure 3.2 and table 3.4, particularly the T_2 and T_1 plots, a growing trend can be noticed since the median values differ and many interquartile ranges only slightly overlap with each other.
The presence of this trend is confirmed for T_2 and partially confirmed for T_1 and D by the results of the Kruskal-Wallis test shown in table 3.5. A p-value lower than 0.05 indicates that the parameters are measured from data sets coming from different populations meaning that they are influenced by something other than the layer they are measured at.
The determination of the factors that influence T_1, T_2 and D is still a subject of study but some hypotheses can be drawn by inspecting figures 3.3 to 3.6 where the parameters are plotted over the total thickness of the sample and each sample's extraction region is indicated. It can be deduced that the values for T_1 and T_2 show a weak correlation with the sample's thickness. This observation is in agreement with the known anatomical notion that some morphological changes of the cartilage are related to the total thickness and thus both the relaxation times T_1 and T_2 show sensitivity to these morphological changes.

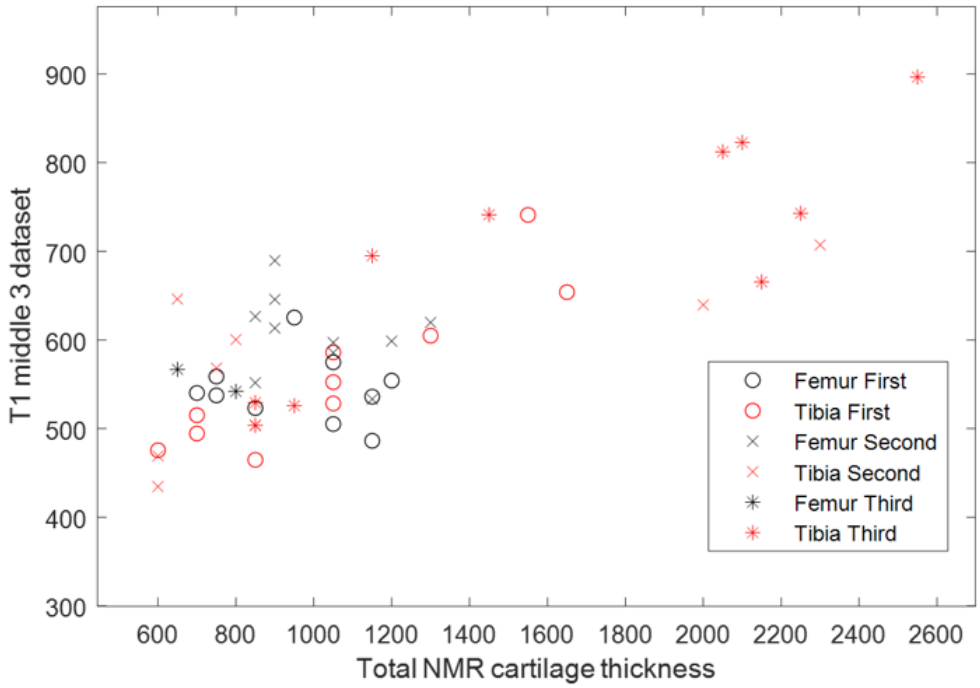

Figure 3.3: *Plotting of T_1 over the total cartilage thickness measured by NMR.*

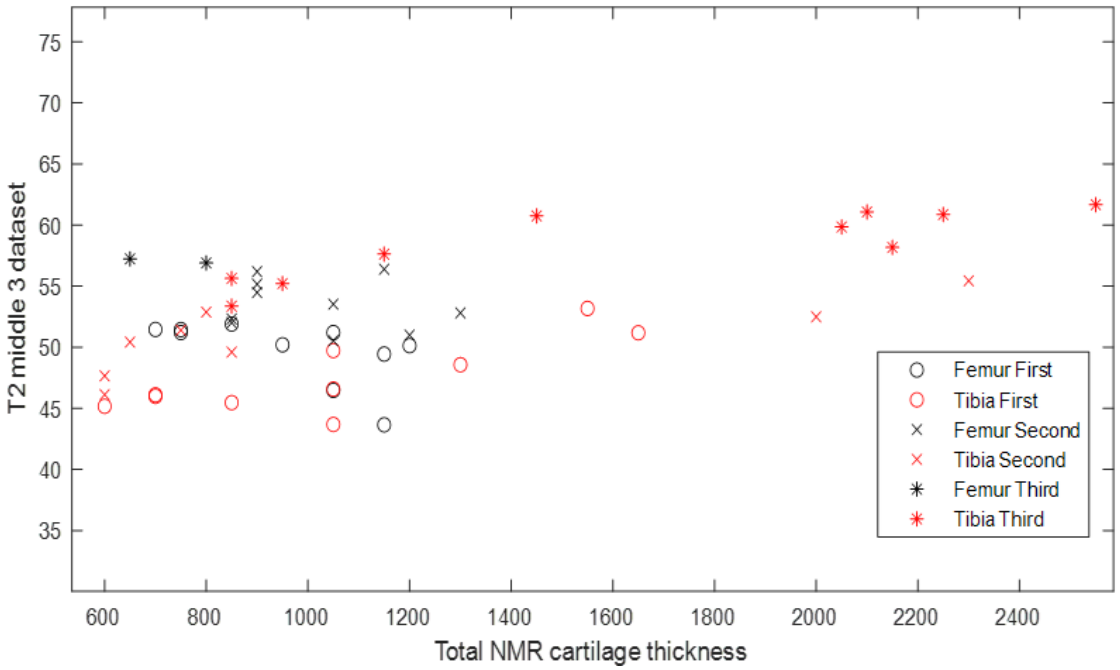

Figure 3.4: *Plotting of T_2 over the total cartilage thickness measured by NMR.*

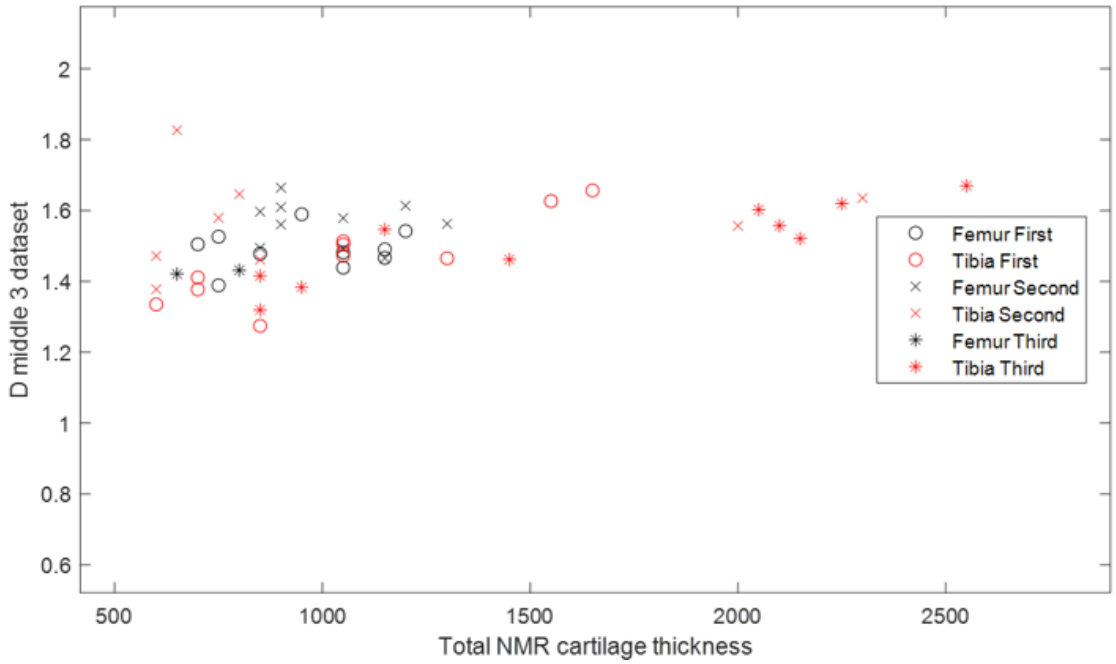

Figure 3.5: *Plotting of D over the total cartilage thickness measured by NMR.*

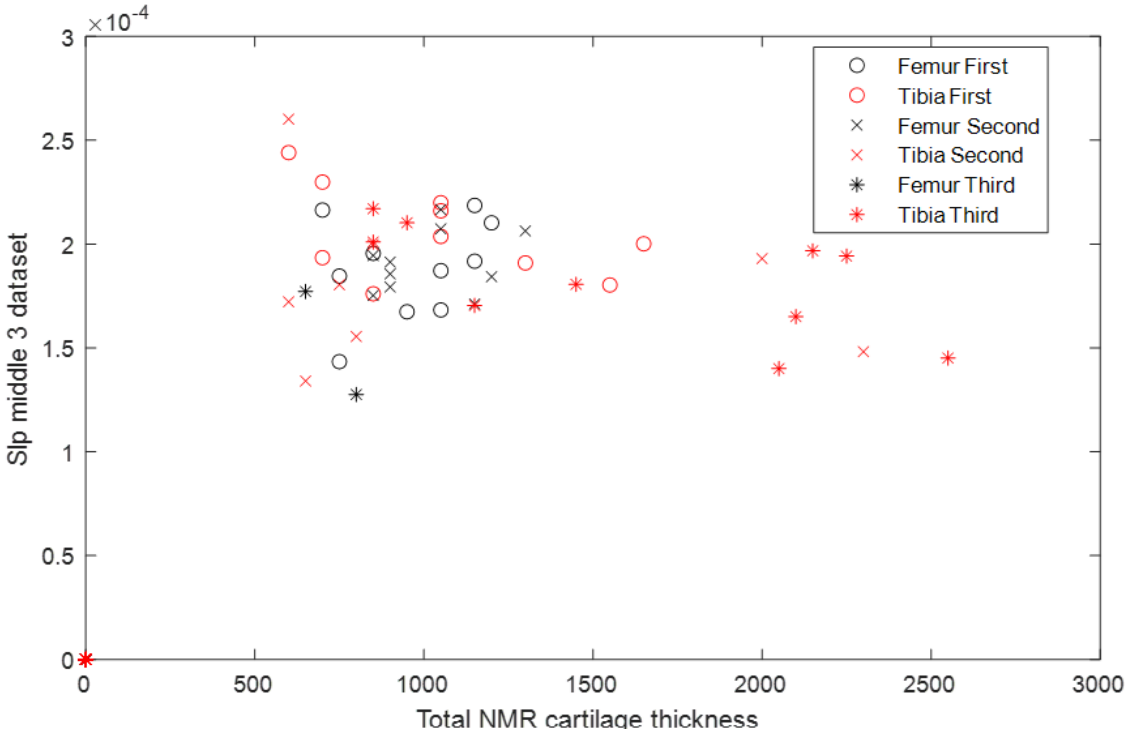

Figure 3.6: *Plotting of α over the total cartilage thickness measured by NMR.*

The values measured for the parameters α and D appear to be much more homogeneous over changes in thickness. The behavior of D can arise from the measurements setup. In fact, the ^1H of water molecules experience a displacement of only few micrometers during the measure, and this diffusion length seems to be ineffective in detecting the kind of morphological changes related to the different thickness of the middle layers considered. The parameter α, on the other hand, is proportional to the ratio between the ^1Hs present in molecules that form solid structures (i.e. low mobility ones) and those in molecules that are in liquid form (i.e. high mobility ones), thus being more sensitive to composition changes rather than morphological ones.

Conclusions

In conclusion, the results of this work demonstrated the capability of low field single sided NMR devices to determine a set of parameters (T_1, T_2, D, α) sensitive to both morphological and compositional changes of the articular cartilage tissue. This possibility paves the way to near future studies which would define the relationship between NMR parameters and the tissue's mechanical properties. Moreover, the study will be developed to assess possible degradation effects on cartilage tissue due to pathologies like osteoarthritis.

The preliminary results, obtained both in this thesis work and in previous measurements, open the possibility for the development of both new NMR techniques and instruments in order to achieve better signal-to-noise ratio and penetration depth in order to study in vivo samples.

The development of new single-sided instruments and techniques, in particular, would have great socio-economic impact since the costs associated are orders of magnitude lower than conventional NMR equipment. This would certainly allow a more capillary diffusion in economically developed countries, but also much greater coverage in economically developing regions.

Appendix A

Signal acquisition

Signal acquisition is dependent on sampling frequency and the acquisition window, i.e. the time window where the radio frequency coil is receptive to signal.
The nomenclature "number of points" is jargon for the product between the two aforementioned quantities. The number of points is the number of times the signal intensity is measured during the acquisition phase of a pulse sequence and it directly influences the quality of the acquired signal as that is taken as the area between the curves of the real and imaginary part of the signal, averaged on the number of points. It is important to note that this procedure allows for a negligible instrument error: the accuracy of a measurement with the NMR-MOUSE can therefore be considered,in a practical context, as only limited by the number of repetitions performed.

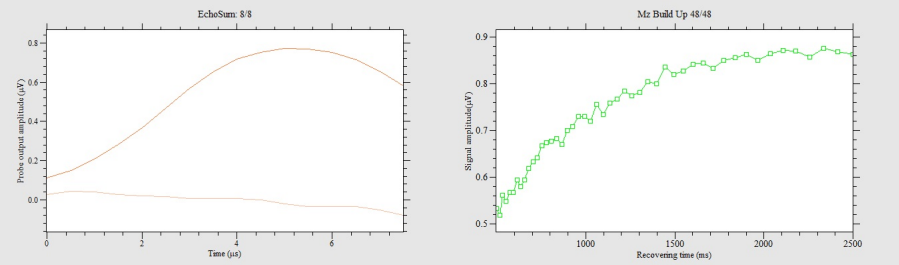

Figure A.1: *Example of a SR sequence as seen in the Prospa software: on the left is shown a single (the last one in the sequence) acquisition. On the right the signal intensity with respect to the recovering time is plotted. A single point in the right plot is acquired by averaging the signal over the number of points, then averaging again over the number of scans.*

Bibliography

[1] Ali Guermazi et al. "Why radiography should no longer be considered a surrogate outcome measure for longitudinal assessment of cartilage in knee osteoarthritis". In: *Arthritis Research and Therapy* 13 (6 Nov. 2011), pp. 1–11. ISSN: 14786354. DOI: 10.1186/AR3488/TABLES/1. URL: https://arthritis-research.biomedcentral.com/articles/10.1186/ar3488.

[2] URL: https://www.healthdata.org/gbd.

[3] Christopher J L Murray. "The Global Burden of Disease Study at 30 years". In: *nature medicine* (2021). DOI: 10.1038/s41591-022-01990-1. URL: https://doi.org/10.1038/s41591-022-01990-1.

[4] Susanne Grässel et al. "Recent advances in the treatment of osteoarthritis". In: (2020). DOI: 10.12688/f1000research.22115.1. URL: https://doi.org/10.12688/f1000research.22115.1.

[5] Emily J Clarke, James R Anderson, and Mandy J Peffers. "Nuclear magnetic resonance spectroscopy of biofluids for osteoarthritis". In: *British Medical Bulletin* 137 (2021), pp. 28–41. DOI: 10.1093/bmb/ldaa037.

[6] David T Felson and Richard Hodgson. "Identifying and Treating Pre-Clinical and Early Osteoarthritis". In: (2014). DOI: 10.1016/j.rdc.2014.07.012.

[7] F. Eckstein et al. "Magnetic resonance imaging (MRI) of articular cartilage in knee osteoarthritis (OA): morphological assessment". In: *Osteoarthritis and Cartilage* 14 (SUPPL. 1 Jan. 2006), pp. 46–75. ISSN: 1063-4584. DOI: 10.1016/J.JOCA.2006.02.026.

[8] Alice J. Sophia Fox, Asheesh Bedi, and Scott A. Rodeo. "The basic science of articular cartilage: Structure, composition, and function". In: *Sports Health* 1 (6 Nov. 2009), pp. 461–468. ISSN: 19417381. DOI: 10.1177/1941738109350438.

[9] Malcolm H. Levitt. *Spin dynamics : basics of nuclear magnetic resonance*. John Wiley & Sons, 2001, p. 686. ISBN: 0-471-48921-2.

[10] M. P. Kennett. *Essential statistical physics*. 2021, p. 250. ISBN: 9781108480789.

[11] Jörg Kärger et al. "Pulsed field gradient NMR diffusion measurement in nanoporous materials". In: *Adsorption* 27 (3 Apr. 2021), pp. 453–484. ISSN: 15728757. DOI: 10.1007/s10450-020-00290-9.

[12] G Eidmann et al. *The NMR MOUSE, a Mobile Universal Surface Explorer*. 1996, pp. 104–109.

[13] S. Meiboom and D. Gill. "Modified spin-echo method for measuring nuclear relaxation times". In: *Review of Scientific Instruments* 29 (8 1958), pp. 688–691. ISSN: 00346748. DOI: 10.1063/1.1716296.

[14] WA Edelstein et al. "Signal, noise, and contrast in nuclear magnetic resonance (NMR) imaging". In: *Journal of computer assisted tomography* (1983), pp. 391–401. URL: https://www.academia.edu/download/54642035/CNRpaper.JCAT1983.pdf.

[15] Wiesmath A. Filip C. Demco D.E. Blumich B. "NMR of Multipolar Spin States Excitated in Strongly Inhomogeneous Magnetic Fields." In: *Journal of Magnetic Resonance* (154 2002).

[16] William H Kruskal and W Allen Wallis. *Use of Ranks in One-Criterion Variance Analysis*. 1952, pp. 583–621.

Ringraziamenti

Ringrazio il professor Brizi e Carlo per avermi permesso di assistere alla realizzazione di un progetto dalle grandi potenzialità grazie al quale ho avuto l'opportunità di comprendere quanto veramente la fisica abbia vastissimi orizzonti e per avermi aiutato a riaccendere una passione per la materia che forse si stava spegnendo.

Ringrazio profondamente i miei genitori, senza i quali questo percorso sarebbe stato impossibile, i nonni e la mia famiglia tutta per essermi stati vicino e per avermi aiutato costantemente.

Ringrazio Sara e Maya per farmi alzare la mattina invece che la sera e per riempire le mie giornate.
Ringrazio Simone e i ragazzi per aver reso piacevole l'esperienza bolognese (!!!).
Ringrazio poi sicuramente Snap e Sant...
...
...
...
...
...
...
... e anche Scara per essere ostaggi compiacenti dei miei vaneggiamenti.
Ringrazio per lo stesso motivo anche il resto dei miei carissimi amici *che non elenco perchè facciamo finta che siano tanti*